ACS OMEGA

Open Access

http://pubs.acs.org/journal/acsodf

Article

Selective Deoxygenation of Waste Cooking Oil to Diesel-Like Hydrocarbons Using Supported and Unsupported $NiMoS_2$ Catalysts

Dechpol Prangklang, Dusadee Tumnantong, Boonyawan Yoosuk, Chawalit Ngamcharussrivichai, and Pattarapan Prasassarakich*

Cite This: *ACS Omega* 2023, 8, 40921−40933

Read Online

ACCESS | Metrics & More | Article Recommendations | Supporting Information

ABSTRACT: This work aimed to study the deoxygenation of two different waste cooking oils (WCOs; palm oil and soybean oil) using alumina (γ-Al_2O_3)-supported and unsupported $NiMoS_2$ catalysts prepared by the hydrothermal method. The variables evaluated in this study were the reactant concentration, reaction time, and nickel (Ni)/[Ni + molybdenum (Mo)] atomic ratio (0.2 and 0.3) affecting the yield and selectivity of alkane products. The supported NiMo sulfide ($NiMoS_2$)/γ-Al_2O_3 catalyst prepared by impregnation had the drawback of a lack of layers and stacks, so combining the γ-Al_2O_3 with unsupported $NiMoS_2$ catalysts using a hydrothermal method was evaluated. The main products obtained from the deoxygenation of the two WCOs were normal (n-)alkane compounds (C_{15}, C_{16}, C_{17}, and C_{18}). The catalyst efficiency was ranked as 0.2-$NiMoS_2$/γ-Al_2O_3 ≈ 0.2-$NiMoS_2$ > 0.3-$NiMoS_2$/γ-Al_2O_3 ≈ 0.3-$NiMoS_2$. The catalyst that gave the high n-C_{15}−C_{18} yield was 0.2-$NiMoS_2$/γ-Al_2O_3 under a reaction condition of 300 °C, 40 bar initial H_2 pressure, and oil concentration of 5 wt %. For the hydrodeoxygenation (HDO) of waste palm oil, the n-C_{14}−C_{18} yield was 56.4% (C_{14}, C_{15}, C_{16}, C_{17}, and C_{18} at 1.3, 6.7, 14.5, 11.8, and 22.1%, respectively), while that for the waste soybean oil was 58% (C_{14}, C_{15}, C_{16}, C_{17}, and C_{18} at 1.1, 3.8, 6.7, 17.2, and 29.2%, respectively). The n-C_{18}/n-C_{17} and n-C_{16}/n-C_{15} ratios were both greater than 1 for both types of WCO, revealing that the deoxygenation mainly proceeded via HDO rather than decarbonylation and decarboxylation. The 5−10% lower n-C_{14}−C_{18} yield from the waste oil compared with the fresh oil was acceptable, implying the effective oil treatment and some impurity removal.

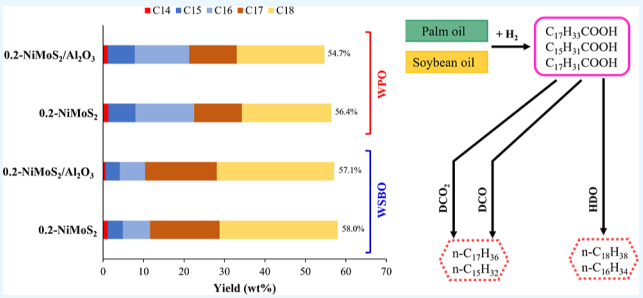

1. INTRODUCTION

The use of transport fuel that is derived from renewable natural resources is highly needed in order to lower greenhouse gas emissions. The most widely used renewable resource is vegetable oil, which is used to produce biodiesel, which is a type of vehicle fuel. Most of the time, edible oils, such as palm oil (PO), soybean oil (SBO), and rapeseed oil, have been used as feedstocks for biodiesel production. However, using biomass resources other than for food is not advised in terms of food security. Vegetable oils are primarily consumed in metropolitan areas, particularly in sectors like households, restaurants, food, and beverage businesses, leading to the production of large quantities of waste oils.[1,2] Although these vegetable oils are edible when fresh, they become toxic and bad for human health after heating above certain temperatures, such as in cooking, and hence become waste oils.

The used (waste) vegetable oil can be a valuable nonfood biomass. At present, waste vegetable oil from the domestic sector and grease from the industrial sector are thrown away in many countries. These low-grade waste oils occasionally contain a large content of free fatty acids (FFAs) and so cannot be readily utilized as feeds in biodiesel production. Thus, hydrodeoxygenation (HDO) is appropriate for transforming the waste vegetable oils into hydrocarbons (HCs), or "second-generation biodiesel", that are comparable to the elements in petroleum fuel. Various crop oils, like PO,[3−5] SBO,[6] rapeseed oil,[7,8] and sunflower oil,[9] have been reported to undergo HDO using supported nickel (Ni) and Ni-molybdenum (Mo) catalysts. The deoxygenation process can produce second-generation biodiesel from various types of vegetable oils and waste oils.

In the deoxygenation process, the vegetable oils lose oxygen atoms from the fatty acids via three types of reactions: HDO, decarbonylation (DCO), and decarboxylation (DCO_2).[5,8,10] The products are normal alkane compounds with carbon atoms between C_{15}−C_{18}, and this type of biodiesel, known as synthetic biohydrogenated diesel (BHD), has the same properties as diesel produced from petroleum.[11,12]

Received: August 21, 2023
Accepted: October 5, 2023
Published: October 20, 2023

Accordingly, the metal catalysts with active phases, such as ruthenium (Ru),[13] rhodium,[14] platinum (Pt),[15] palladium (Pd),[16] and Ni,[17] were used in oil hydrotreating. However, the HDO reaction is catalyzed less efficiently over time than the DCO and DCO_2 reactions. Moreover, several metals, including Pt, Pd, and Ni, that have the capacity to accelerate the methanation reaction require a significant amount of hydrogen (H_2) gas, which is inappropriate for this process. Consequently, bimetallic catalysts with multiple active phases, like NiMo disulfide ($NiMoS_2$)[18,19] and cobalt (Co)MoS_2,[19,20] can speed up the HDO reaction and make it more effective than the DCO and DCO_2 reactions. The Ni and Co promoters catalyze the hydrogenation of alkenes to alkanes.

Heterogenous catalysts generally require a good support as an inert substance that acts to disperse the activated metal to increase its stability by reducing sintering when used at high temperatures and to increase the active surface area in catalysis. There are many types of suitable supports, such as the metal oxides [alumina (γ-Al_2O_3), titania (TiO_2), and magnesium oxide], silica (SiO_2), zeolite, and activated carbon (AC),[21−23] that have a high surface area and porosity, and their selection depends on the application and inertness to unwanted reactions. A good support needs to be stable under active and reusable conditions of the catalyst, while the high surface area results from the small pores but clogging can occur within very small pores.

For the addition of a promoter to raise the catalyst activity in the deoxygenation process, Co or Ni are frequently added to the catalyst to improve the catalytic HDO reaction.[19,24] Previous research has shown that unsupported bimetallic Ni−Mo and Co−Mo catalysts were efficient for the oleic and palmitic acid HDO, where the bimetallic Ni−Mo catalyst gave a mainly alkane product (mostly containing n-C_{15}−C_{18}).[19] For the creation of PO-derived BHD, $NiMoS_2/\gamma$-Al_2O_3 was an efficient catalyst for four cycles of the HDO of PO allowing the catalyst to be recycled.[18] A comparison of different metal catalysts in the deoxygenation of SBO revealed a ranked SBO conversion (highest to lowest) of: NiMo > Pd > CoMo > Ni > Pt > Ru.[6]

Herein, some selected works on the catalytic HDO of oils using catalysts with different supports are briefly reviewed. For the deoxygenation of palmitic acid using Ni catalysts with different supports [zirconia (ZrO_2), H-ZSM-5, and AC] prepared by wet impregnation, the Ni/H-ZSM-5 and Ni/ZrO_2 catalysts gave 86 and 93% conversions, respectively.[25] The deoxygenation of PO using a Ni−MoS_2/Al_2O_3 catalyst resulted in the HDO reaction being mainly responsible for the 92 wt % product yield.[26] In contrast, deoxygenation of PFAD using a Pd/C catalyst proceeded via the DCO pathway as the main reaction route and the reusability of the regenerated and unremediated Pd/C catalysts gave a much lower conversion and HC product yield in the second use compared to in the first use.[27] For deoxygenation of PO using a Ni/SAPO-11 catalyst, the addition of Ni metal in different proportions yielded different percentages of n-alkanes.[3]

With respect to supports, the Ni−Mo−W(5−5−15)/γ-Al_2O_3-ZSM-5 (85−15) catalyst prepared by extrusion was found to be efficient for PO deoxygenation,[4] while unsupported $NiMoS_2$ and supported $NiMoS_2/\gamma$-Al_2O_3 catalysts gave a sufficiently high yield of alkanes (n-C_{14}−C_{18}).[28] Interestingly, the hydrothermal catalytic deoxygenation using a simple Ni/ZrO_2 catalyst was found to be a successful method for eliminating oxygen from palmitic acid.[29] Thus, the catalyst should be designed with the appropriate metals, promoters, supports, and compositions depending on the type of vegetable oil feedstock.

In this work, two types of waste cooking oil (WCO) as a renewable feedstock were used in comparison to the equivalent fresh oil. These were fresh (F) and waste (W)PO and FSBO and WSBO. The WPO consisted of 40.8 wt % palmitic acid and 45.2 wt % oleic acid while the WSBO consisted of 53.0 wt % linoleic acid, 24.5 wt % oleic acid, and 11.5 wt % palmitic acid as the main components.[30,31] Previous research established the efficiency of Ni, rather than Pt, Pd, and Co as the metal promoter and of γ-Al_2O_3 as the support rather than ZrO_2, SiO_2, ZSM-5, and SAPO-11. Thus, they were chosen due to their low cost and straightforward catalyst synthesis (without sulfidation), which are important traits for scale-up and potential production. The deoxygenation of the fresh and waste vegetable oils (FSBO, WSBO, FPO, and WPO) was evaluated using supported $NiMoS_2/\gamma$-Al_2O_3 and unsupported $NiMoS_2$ catalysts prepared by hydrothermal synthesis, and the effect of Ni/(Ni + Mo) ratio, waste oil type, and conditions (reaction time and oil concentration) on C_{14}, C_{15}, C_{16}, C_{17}, and C_{18} n-alkane yield was reported. The physical characterization of the catalysts was performed to understand their activity affecting the C_{14}−C_{18} product yield.

2. EXPERIMENTAL SECTION

2.1. Materials. Ammonium tetra thiomolybdate [ATTM; $(NH_4)_2MoS_4$, Sigma-Aldrich], nickel nitrate hexahydrate [$Ni(NO_3)_2{\cdot}6H_2O$; Sigma-Aldrich], decahydronaphthalene (decalin, Fluka), n-decane (Sigma-Aldrich), and γ-Al_2O_3 (0.06−0.2 mm diameter, Merck) were used as received. The FPO and FSBO were from a supermarket, while the crude (c) WPO was from a local restaurant and the cWSBO was from a house.

2.2. Catalyst Synthesis.

1 For the synthesis of unsupported $NiMoS_2$ catalyst by the hydrothermal method,[32,33] 0.3 g of ATTM was dissolved in 50 g of deionized water, mixed with $Ni(NO_3)_2{\cdot}6H_2O$ (dissolved in a small amount of water), and then 5 g of decalin was added. A 250 mL Parr reactor was charged with the mixed solution, pressurized to a 28 bar initial H_2 pressure (P_{H_2}), and heated to 360 °C for 60 min. The catalysts were designated as 0.2-$NiMoS_2$ and 0.3-$NiMoS_2$ for Ni/(Ni + Mo) atomic ratios of 0.2 and 0.3, respectively.
2 For the synthesis of supported $NiMoS_2$ catalyst using the hydrothermal method, ATTM and $Ni(NO_3)_2{\cdot}6H_2O$ were dissolved in deionized water.[28] The solution with decalin added was heated at 80 °C for 30 min and then, γ-Al_2O_3 (20 wt % loading based on the catalyst weight) was added. The catalyst was synthesized in a Parr reactor at 350 °C and 28 bar initial P_{H_2}. The catalysts were designated as 0.2-$NiMoS_2/\gamma$-Al_2O_3 and 0.3-$NiMoS_2/\gamma$-Al_2O_3 for Ni/(Ni + Mo) atomic ratios of 0.2 and 0.3, respectively.

2.3. Catalyst Characterization. The nitrogen (N_2) adsorption−desorption profiles of catalyst were measured using a Micromeritics ASAP-2020 surface area and porosity analyzer to derive the Brunauer−Emmett−Teller (BET) surface area (S_{BET}), while the total pore volume (V_p) and average pore diameter were evaluated using the Barrett−Joyner−Halenda method. The X-ray diffraction (XRD)

https://doi.org/10.1021/acsomega.3c06188
ACS Omega 2023, 8, 40921−40933

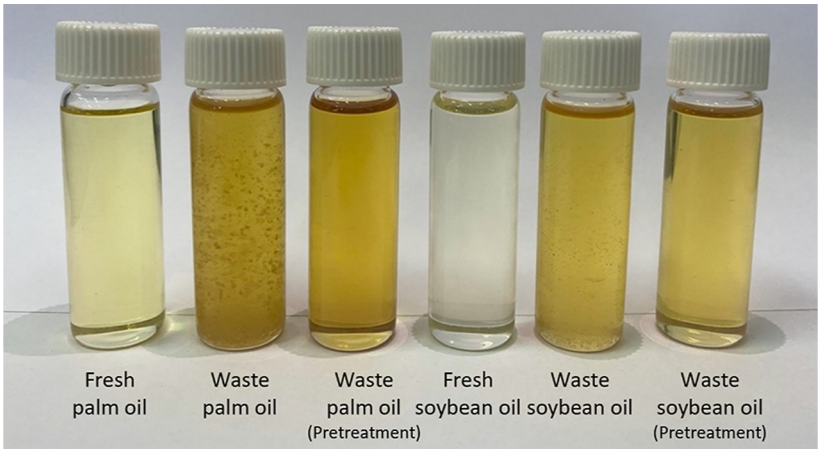

Figure 1. Representative images of fresh, crude waste, and pretreated waste PO and SBO. (Photograph courtesy of "Dechpol Prangklang". Copyright 2022).

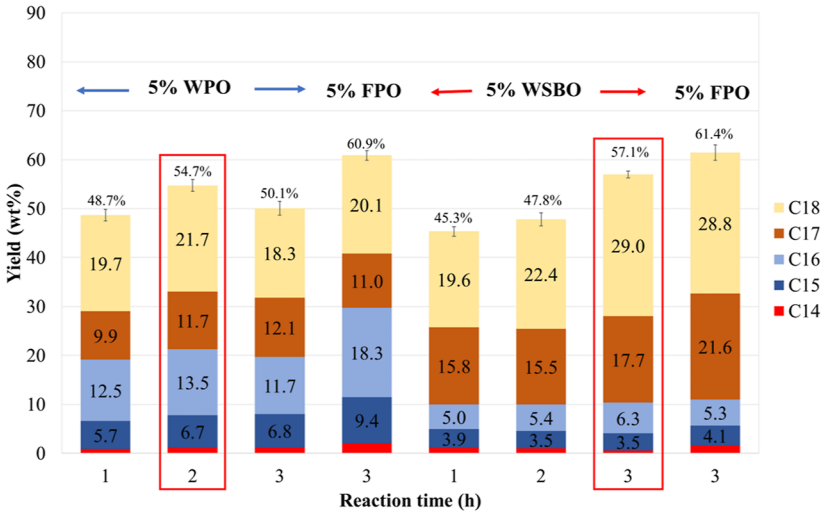

Figure 2. Deoxygenation of fresh and waste oils (FPO, WPO, FSBO, and WSBO) over the unsupported 0.2-$NiMoS_2$ catalyst at various times. Condition: 300 °C, 40 bar P_{H_2}, and 5 wt % oil concentration.

patterns were recorded on a Bruker AXS-D8 Discover X-ray diffractometer with Cu Kα emission (λ = 1.5406 Å) operating at 40 kV and 40 mA.

The surface morphology of catalysts was examined by transmission electron microscopy/energy-dispersive X-ray spectroscopy (TEM/EDX) using a JEM 2100 Plus JEOL transmission electron microscope. A sample suspension drop was placed on a carbon film supported by a copper grid. For determining the acid properties of catalyst, temperature-programmed desorption of ammonia (NH_3-TPD) was recorded on a BELCAT-B instrument. The sample was heated to 500 °C, then cooled to room temperature, and reheated to 500 °C with introducing 10 vol % NH_3/He. Thermal conductivity detector was used for effluent gas analysis.

2.4. Pretreatment of the cWCOs. For the pretreatment of the obtained cWCOs, they were filtered to remove waste residue, centrifuged to bring the oil layer to bubble by the washing technique (hot water extraction method), and then blown by air to bubble in the separation funnel so that the FFAs came out of the oil layer.[34] The water/oil mixture was set aside to allow phase separation, resulting in three phases (water, FFAs, and oils). Finally, the oil layer was removed and evaporated to obtain the oil without FFAs and used as the pretreated WCO (hereafter termed simply WCO, WPO, and WSBO) in the subsequent deoxygenation. The appearances of the fresh, crude waste, and pretreated-waste palm and soybean oils are shown in Figure 1.

2.5. Deoxygenation of the FCOs and WCOs: HDO Reaction. For deoxygenation of the FCOs and WCOs, the Parr reactor was charged with 1.0−2.0 g of the respective fresh oil (FPO or FSBO) or pretreated WCO (WPO or WSBO), 18 g of *n*-decane, and 0.22−0.33 g of catalyst, pressurized to 40 bar initial P_{H_2} (H_2 purity >99.995%), and heated to 300 °C (oil concentrations of 5 and 10 wt % and catalyst/oil ratios of 0.15 and 0.1 for the supported and unsupported $NiMoS_2$ catalysts, respectively). After the reaction, the gas was released from the cooled reactor, and the liquid products and the catalyst powder were separated.

2.6. Analysis of the Alkane Products and Byproducts. The fresh and waste oils (FPO, WPO, FSBO, and WSBO) before and after the deoxygenation reaction were examined by attenuated total reflectance Fourier-transform infrared spectroscopy (ATR-FTIR; Thermo Fisher model: Nicolet IS5).

The liquid product was analyzed using gas chromatography (GC) with a flame ionization detector (FID; Shimadzu GC2010) and an HP-88 column (L = 100 m, Ø = 0.25 mm,

https://doi.org/10.1021/acsomega.3c06188
ACS Omega 2023, 8, 40921−40933

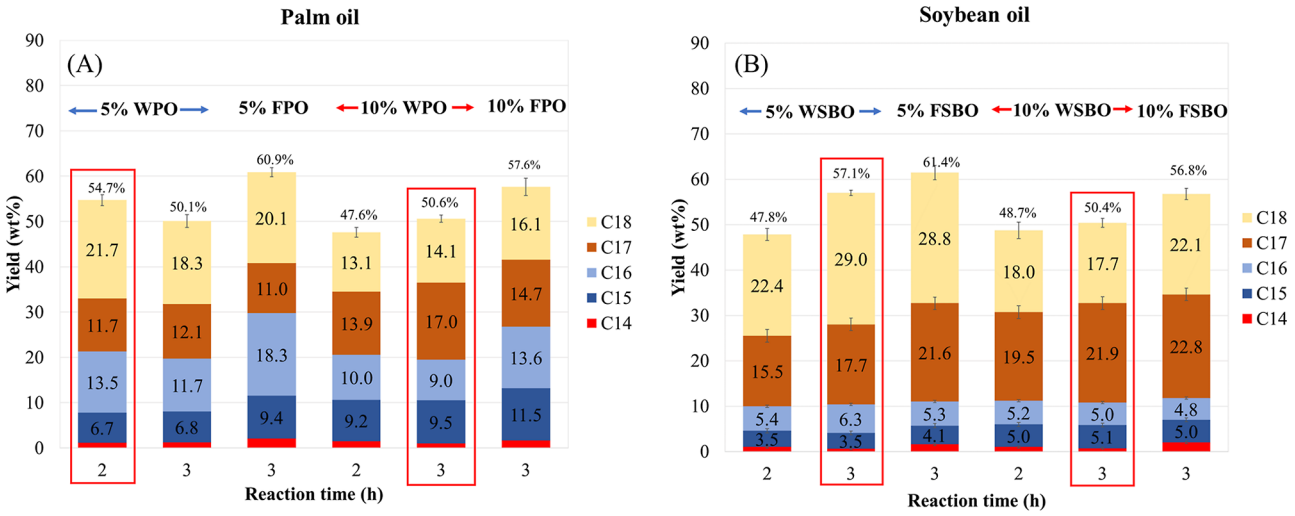

Figure 3. Deoxygenation of (A) FPO and WPO and (B) FSBO and WSBO over the unsupported 0.2-$NiMoS_2$ catalyst at different oil concentrations. Condition: 300 °C, 40 bar of P_{H_2}, and a catalyst/oil ratio of 0.1.

and film thickness = 0.2 μm). The carrier gas was helium (He) at a flow rate of 1.24 mL/min. The sample solution was injected at a split ratio of 100:1. Representative chromatograms presenting the C_{14}, C_{15}, C_{16}, C_{17}, and C_{18} peaks from the deoxygenation of the WPO and WSBO are shown in Figure S1, with the retention times, as shown in Table S1. The liquid product was also analyzed by GC/mass spectroscopy (GC/MS; Shimadzu GCMS-QP2010) equipped with a DB-1 column (L = 60 m, Ø = 0.25 mm, film thickness = 0.2 μm). The He flow rate was 1.24 mL/min. The sample solution was injected at a split ratio of 100:1 and the m/z was 35−600.

3. RESULTS AND DISCUSSION

3.1. Deoxygenation of the Oils Using an Unsupported Ni−Mo Catalyst. In this work, the reaction time and oil concentration were the studied variables that affect the deoxygenation of the oils via the HDO, DCO, DCO_2, isomerization, and hydrocracking reactions. The n−C14−C18 yield and selectivity at various times (1−3 h) are presented in Figure 2 and Table S2. The reaction was performed at 300 °C, 40 bar initial P_{H2}, and 5 wt % oil concentration as this was reported to be the optimum condition.[19,28,32]

3.1.1. Influence of the Oil Concentration and Time. For the deoxygenation of the WPO (Figure 2), after a 1 h reaction time, the n−C14−C18 yield was high at 48.7%, indicating that the unsupported 0.2-$NiMoS_2$ catalyst prepared via the hydrothermal synthesis from ATTM was effective. Increasing the reaction time from 1 to 2 h increased the n-C_{14}−C_{18} yield to a maximum of 54.7% (C_{14}, C_{15}, C_{16}, C_{17}, and C_{18} at 1.1, 6.7, 13.5, 11.7, and 21.7%, respectively) and then decreased at 3 h to 50.1%. Thus, the initial reaction rate (1 h) was high and thereafter decreased, approaching equilibrium. The optimum reaction time for the deoxygenation of WPO was 2 h, based upon the highest n-C_{14}−C_{18} yield and selectivity (Figure 2 and Table S2). In Table S2, the n-C_{18}/n-C_{17} and n-C_{16}/n-C_{15} ratios were in the range of 1.5−2.2 at 1−3 h, implying that HDO was the main reaction pathway rather than DCO and DCO_2.

For the deoxygenation of WSBO (Figure 2), the n-C_{14}−C_{18} yield after 1 h was also high at 45.4%, similar to the deoxygenation of WPO, but the n-C_{14}−C_{18} yield further increased to a maximum yield of 57.1% after 3 h (C_{14}, C_{15}, C_{16}, C_{17}, and C_{18} = 0.6, 3.5, 6.3, 17.7, and 29.0%, respectively). Thus, the 0.2-$NiMoS_2$ catalyst gave a high reaction rate in the first hour, and the reaction rate decreased in the period of 1−3 h and began to reach equilibrium. The optimum time for HDO of WSBO was 3 h, at which the highest n-C_{14}−C_{18} yield and selectivity were achieved (Figure 2 and Table S2). In the same manner as for the deoxygenation of WPO, the n-C_{18}/n-C_{17} and n-C_{16}/n-C_{15} ratios were in the range of 1.2−1.8 at 1−3 h (Table S2), indicating that the HDO reaction occurred rather than the DCO_2 and DCO pathways.

The n-C_{14}−C_{18} product yield and selectivity from the deoxygenation at different oil concentrations (5−10 wt %) are presented in Figure 3 and Table S2. For WPO, the n-C_{14}−C_{18} yield and selectivity decreased with increasing oil concentrations. The n-C_{14}−C_{18} yield after 2 h was decreased from 54.7% at 5 wt % oil to 47.6% (C_{15}, C_{16}, C_{17}, and C_{18} = 9.2, 10, 13.9, and 13.1%, respectively) at 10 wt % oil, although at this higher oil concentration it was maximal after 3 h at 50.6%.

For the deoxygenation of WSBO, at the optimal time (3 h), the n-C_{14}−C_{18} yield was also decreased from 57.0% at 5 wt % oil to 50.4% (C_{15}, C_{16}, C_{17}, and C_{18} = 5.1, 5.0, 21.9, and 17.7%, respectively) at 10 wt % oil. The n-C_{14}−C_{18} yield and selectivity decreased at a high oil concentration due to the lower rate of H_2 and oil diffusion to the surface of catalyst resulting in a decreased catalyst efficiency and HDO rate (Figure 3). Thus, the optimum concentration (low) promoted the deoxygenation of the oil via the HDO reaction rather than the DCO_2 and DCO pathways, and so the n-C_{18}/n-C_{17} and n-C_{16}/n-C_{15} ratios were above 1 (1.3−2.2) (Table S2). Whereas, at a higher oil concentration (10 wt %), the n-C_{18}/n-C_{17} and n-C_{16}/n-C_{15} ratios were in the range of 0.9−1.1 (Table S2) implying that the DCO_2 and DCO reactions occurred equally with HDO.

A possible explanation for the effect of the oil concentration on the n-C_{14}−C_{18} product yield and selectivity in the deoxygenation process is as follows. When the oil concentration was increased from 5 to 10 wt %, the n-C_{14}−C_{18} yield and the selectivity of the C_{16} and C_{18} products tended to decrease because a high oil concentration caused (i) an increased viscosity, (ii) low free volume, and (iii) decreased diffusion rate of the H_2 and oil at the catalyst surface. Thus, the

https://doi.org/10.1021/acsomega.3c06188
ACS Omega 2023, 8, 40921−40933

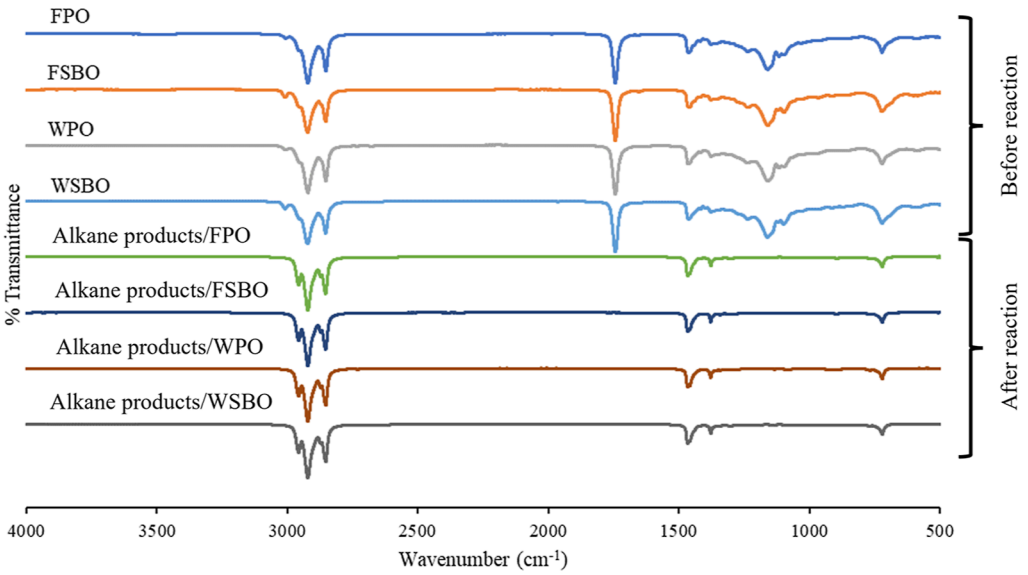

Figure 4. Representative FTIR spectra of fresh and waste oils (FPO, WPO, FSBO, and WSBO) before and after the deoxygenation reaction. Alkane products/FPO = alkane products from deoxygenation of FPO at 5% oil concentration using the 0.2-$NiMoS_2$ catalyst.

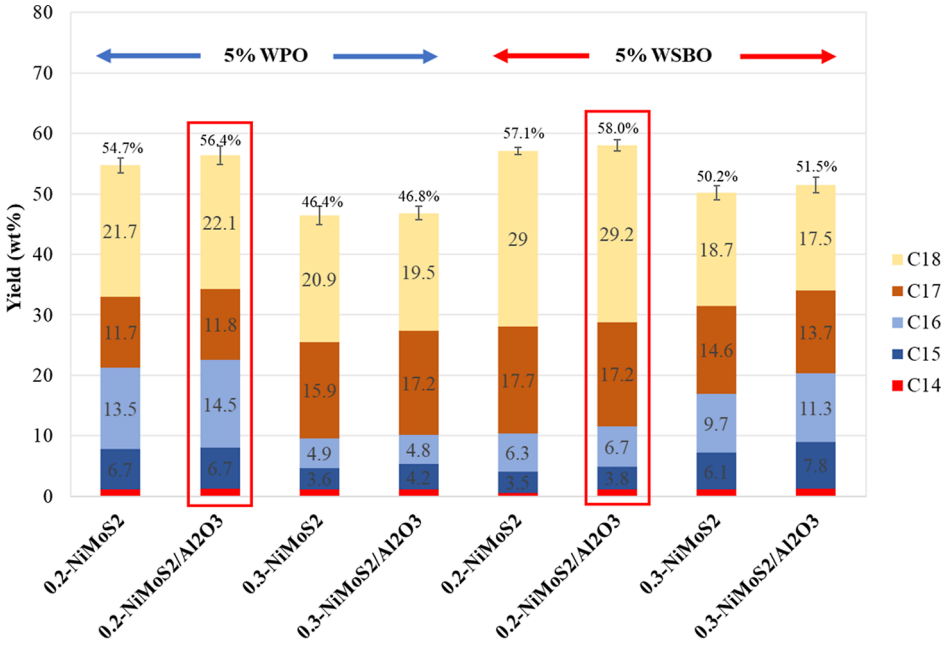

Figure 5. Comparison of the effectiveness of the γ-Al_2O_3-supported and unsupported $NiMoS_2$ catalysts in the deoxygenation of WPO and WSBO. Condition: 300 °C, 40 bar P_{H_2}, reaction time of 3 h, and oil concentration of 5 wt %.

catalyst efficiency was decreased, resulting in the decreased HDO rate.[28]

3.1.2. Comparison of the Deoxygenation of WPO and WSBO. Generally, the oil source is also a variable in the deoxygenation of oils that affects the *n*-alkane yield and selectivity. The deoxygenation of the WPO and WSBP were compared at their optimum reaction conditions, revealing that the *n*-C_{17}−C_{18} yield from WSBO (46.7%) was much higher than that from WPO (33.4%), while the *n*-C_{15}−C_{16} yield from WSBO (9.8%) was much lower that from WPO (20.2%). This was related to the composition of the WPO, which contained palmitic acid and oleic acid at 40.8 and 45.2%, respectively, whereas the WSBO contained palmitic acid, oleic acid, and linoleic acid at 11.5, 24.5, and 53.0%, respectively.[30,31] In summary, deoxygenation of WSBO gave a higher *n*-C_{17}−C_{18} yield (39.6−46.7%) than WPO (30.4−33.4%) but a lower *n*-C_{15}−C_{16} yield (8.2−9.8%) than WPO (18.5−20.2%) (Table S2). It is worth nothing that WPO gave higher *n*-C_{18}/*n*-C_{17} and *n*-C_{16}/*n*-C_{15} ratios than WSBO relating fatty acid structure (saturated vs unsaturated ones).

Comparison of the *n*-C_{14}−C_{18} yield from the deoxygenation of the waste and fresh oils at their respective optimum reaction revealed that the *n*-C_{14}−C_{18} yield from WPO and WSBO (54.7 and 57.1%, respectively) was slightly lower than that from FPO and FSBO (60.9 and 61.4%, respectively) (Figure 2, Table S2). This 5−10% lower *n*-C_{14}−C_{18} yield from the waste oil compared with the fresh oil was acceptable, implying that the effective oil treatment could improve the waste oil

https://doi.org/10.1021/acsomega.3c06188
ACS Omega 2023, 8, 40921−40933

Table 1. Comparison of the Effectiveness of the Supported and Unsupported $NiMoS_2$ Catalysts in the Deoxygenation of WPO and WSBO[a]

oil	WPO			WSBO				
catalyst	0.2-$NiMoS_2$	0.2-$NiMoS_2$ /Al_2O_3	0.3-$NiMoS_2$	0.3-$NiMoS_2$ /Al_2O_3	0.2-$NiMoS_2$	0.2-$NiMoS_2$/Al_2O_3	0.3-$NiMoS_2$	0.3-$NiMoS_2$ /Al_2O_3
time (h)	2	3	3	3	3	3	3	3
n-alkane content (wt %)	54.7	56.4	46.4	46.8	57.1	58	50.2	51.5
	yield (wt %)				yield (wt %)			
C_{14}	1.1	1.3	1.1	1.1	0.6	1.1	1.1	1.2
C_{15}	6.7	6.7	3.6	4.2	3.5	3.8	6.1	7.8
C_{16}	13.5	14.5	4.9	4.8	6.3	6.7	9.7	11.3
C_{17}	11.7	11.8	15.9	17.2	17.7	17.2	14.6	13.7
C_{18}	21.7	22.1	20.9	19.5	29	29.2	18.7	17.5
	selectivity (%)				selectivity (%)			
C_{14}	2.1	2.3	2.3	2.4	1.1	1.9	2.2	2.2
C_{15}	12.2	11.8	7.8	8.9	6.1	6.5	12.2	15.2
C_{16}	24.6	25.7	10.6	10.3	11	11.5	19.4	21.9
C_{17}	21.4	21	34.2	36.8	31	29.7	29	26.7
C_{18}	39.7	39.2	45.1	41.6	50.8	50.4	37.2	34
C_{16}/C_{15}	2.0	2.2	1.4	1.2	1.8	1.8	1.6	1.4
C_{18}/C_{17}	1.9	1.9	1.3	1.1	1.6	1.7	1.3	1.3

[a]Conditions: 300 °C, 40 bar P_{H_2}, and 5 wt % oil concentration.

properties and some impurities could be removed or not poison the unsupported 0.2-$NiMoS_2$ catalyst.

Representative FTIR spectra of fresh and waste oils before and after the deoxygenation reaction are shown in Figure 4. For the fresh and waste oils before the reaction, the absorbance at 2920 and 2852 cm^{-1} was assigned to C−H stretching of hydrocarbon. The absorption bands at 1743 and 1464 cm^{-1} were attributed to C═O stretching and C−H aliphatic bending, respectively. The band at 1156 cm^{-1} corresponded to the C−O stretching vibration of the ester group. Furthermore, the spectra of FPO, WPO, FSBO, and WSBO exhibited similar patterns. For the fresh and waste oils after the reaction, the absorption bands of C═O stretching and C−O ester groups disappeared due to deoxygenation reaction and their peaks also appeared in a similar pattern. The comparison of the *n*-C_{14}−C_{18} yield from the deoxygenation of the waste and fresh oils revealed that the *n*-C_{14}−C_{18} yield from WPO and WSBO was slightly lower than that from FPO and FSBO. This 5−10% lower *n*-C_{14}−C_{18} yield from the waste oil compared with the fresh oil was due to the degradation and cracking during cooking, loss of FFA, and some impurity. However, from FTIR spectra, the FPO and FSBO had a similar triglyceride structure to WPO and WSBO. The alkane products from deoxygenation of FPO, FSBO, WPO, and WSBO had a similar alkane structure via elimination of oxygen from FCO and WCO.

3.2. Deoxygenation of the Oils over a Supported $NiMoS_2$ Catalyst. The supported $NiMoS_2/\gamma$-Al_2O_3 catalyst prepared by impregnation has the drawback of being without layers and stacks, but this could be solved by combining the γ-Al_2O_3 with the unsupported $NiMoS_2$ catalysts in a hydrothermal method.[28] The γ-Al_2O_3-supported and unsupported $NiMoS_2$ catalysts (using the hydrothermal synthesis) with Ni/(Ni + Mo) ratios of 0.2 and 0.3 (0.2-$NiMoS_2$, 0.3-$NiMoS_2$, 0.2-$NiMoS_2/\gamma$-Al_2O_3, and 0.3-$NiMoS_2/\gamma$-Al_2O_3) were evaluated in the deoxygenation of WPO and WSBO. The supported $NiMoS_2/\gamma$-Al_2O_3/WCO ratio and unsupported $NiMoS_2$/WCO was 0.15 and 0.1, respectively. The catalyst types affecting the *n*-C_{14}−C_{18} yield and selectivity are presented in Figure 5 and Table 1.

The removal of oxygen from the fatty acids in the WCOs was followed by means of the *n*-C_{14}−C_{18} product yield in the deoxygenation of WPO and WSBO under the same conditions. It has previously been shown that catalysts supported with γ-Al_2O_3 have a high surface area and an increased dispersion of active metal, while the addition of Ni as a promoter gives a higher ability to remove oxygen from fatty acid molecules than without the promoter.[19,32] Therefore, the addition of appropriate amounts of nickel [as the Ni/(Ni + Mo) ratio] would increase the rate of HDO of fatty acids.[19]

For the deoxygenation of the WPO and WSBO at 5 wt %, the 0.2-$NiMoS_2/\gamma$-Al_2O_3 catalyst gave the highest *n*-C_{14}−C_{18} yield at 56.4% (Figure 5 and Table S3) and 58.0% (Figure 5 and Table S4), respectively. In accordance, the addition of γ-Al_2O_3 at an appropriate amount (20 wt %) was seen to increase the HDO of WPO.[28] Thus, the γ-Al_2O_3-supported $NiMoS_2$ with an optimum Ni/(Ni + Mo) ratio enhanced the HDO of WSBO and WPO.

For the unsupported and γ-Al_2O_3-supported $NiMoS_2$ catalysts with Ni/(Ni + Mo) atom ratios of 0.2 compared with 0.3, the 0.2-$NiMoS_2$ catalyst increased the HDO rate of oleic, palmitic, and linoleic acids, whereas at a higher Ni/(Ni + Mo) ratio of 0.3, there was a clear trend of decreasing the *n*-C_{14}−C_{18} yield (about 8 and 7% for the WPO and WSBO, respectively) and selectivity. The excess Ni atom which might be in the separate phases of the Ni sulfide atoms has the potential to agglomerate and partly block the more active phase of $NiMoS_2$ leading to a decrease in the catalyst efficiency. The catalyst efficiency was ranked (highest to lowest) as 0.2-$NiMoS_2/\gamma$-Al_2O_3 ≈ 0.2-$NiMoS_2$ > 0.3-$NiMoS_2/\gamma$-Al_2O_3 ≈ 0.3-$NiMoS_2$. In the same manner, for fresh oil deoxygenation, the catalyst with the activity ranked as 0.2-$NiMoS_2/\gamma$-Al_2O_3 (63.3%) ≈ 0.2-$NiMoS_2$ (61.4%) > 0.3-$NiMoS_2/\gamma$-Al_2O_3 (57.2%) ≈ 0.3-$NiMoS_2$ (56.4%) (the value in parentheses is *n*-C_{14}−C_{18} yielded from FSBO deoxygenation, as presented in Table S4).

https://doi.org/10.1021/acsomega.3c06188
ACS Omega 2023, 8, 40921−40933

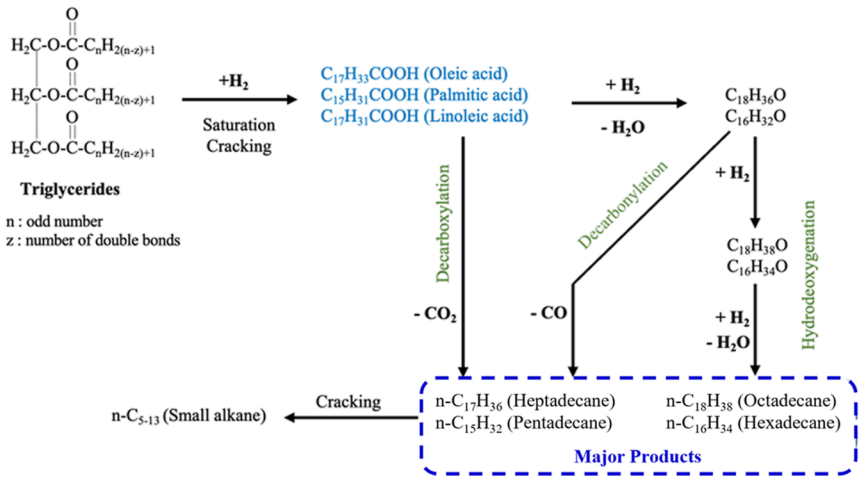

Figure 6. Reaction pathways for the deoxygenation of triglycerides.

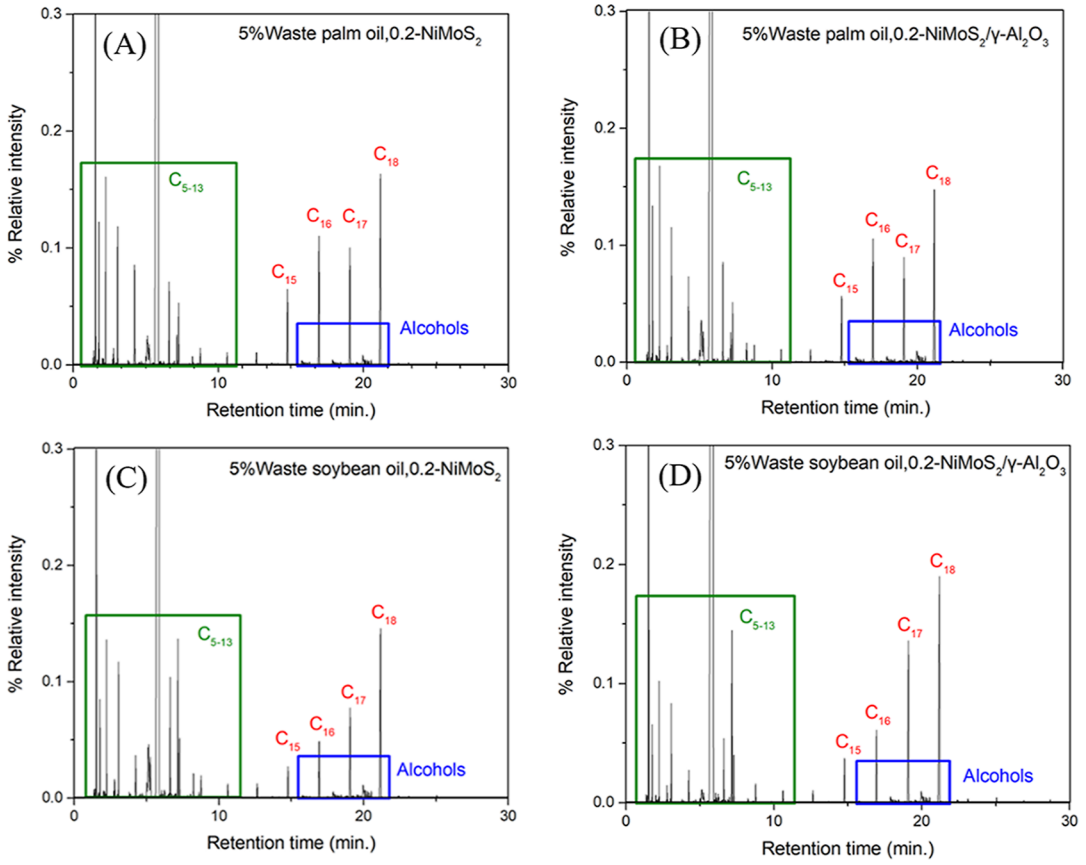

Figure 7. Representative GC/MS chromatograms of the alkane products and byproducts for the deoxygenation of (A,B) WPO and (C,D) WSBO over the (A,C) 0.2-$NiMoS_2$ and (B,D) 0.2-$NiMoS_2/\gamma$-Al_2O_3 catalysts. Condition: 300 °C, 40 bar P_{H_2}, and a catalyst/WCO ratio of 0.1−0.15.

3.3. Analysis of the Alkane Products and Byproducts.

The mechanism of the deoxygenation of WCOs is shown in Figure 6. Initially, unsaturated triglycerides are hydrogenated to saturated triglycerides and then cracked to form fatty acids and propane. For the HDO of FFAs, the main products are normal alkanes, hexadecane (n-C_{16}) and octadecane (n-C_{18}), from both WPO (palmitic and oleic acids) and WSBO (linoleic, oleic, and palmitic acids). For the DCO and DCO_2 of palmitic, oleic, and linoleic acids, pentadecane (n-C_{15}) and heptadecane (n-C_{17}) are formed where the oxygen atoms are removed via the formation of water, carbon monoxide, and carbon dioxide, corresponding to the deduction of one carbon atom. The deoxygenation involves both series and parallel reactions that give the byproducts and intermediates. The main products found were n-C_{15}−C_{18} with minor products of: (i) alcohols, formed from the hydrogenation reaction of aldehydes and esters (formed by the reaction between fatty acids and long-chain alcohols) and (ii) low-molecular-weight normal alkanes (n-C_5−C_{13}), formed from the cracking of high-molecular mass alkanes.

The results of this study on the deoxygenation of WPO and WSBO are consistent with the reaction pathway for triglyceride

https://doi.org/10.1021/acsomega.3c06188
ACS Omega 2023, 8, 40921−40933

Table 2. Components of Observed Biodiesel from the Deoxygenation of WPO and WSBO Over the Supported and Unsupported $NiMoS_2$ Catalysts[a]

oil	WPO				WSBO			
catalyst	0.2-$NiMoS_2$	0.2-$NiMoS_2$ /Al_2O_3	0.3 $NiMoS_2$	0.3-$NiMoS_2$ /Al_2O_3	0.2-$NiMoS_2$	0.2-$NiMoS_2$ /Al_2O_3	0.3-$NiMoS_2$	0.3-$NiMoS_2$ /Al_2O_3
time (h)	2	3	3	3	3	3	3	3
	area (%)				area (%)			
				Alkane				
pentane	0.2	0.2	0.4	0.2	0.2	0.1	0.2	0.2
hexane	3.6	4.2	5.1	5.0	2.7	2.0	3.7	5.3
heptane	5.3	6.1	6.8	6.9	4.6	3.2	5.3	7.3
octane	4.7	5.5	5.9	6.0	5.0	3.2	0.9	0.6
nonane	5.0	5.6	5.2	5.6	4.3	1.4	4.1	2.8
undecane	2.0	1.5	4.8	4.2	8.0	8.1	1.3	1.6
dodecane	0.1	0.2	0.1	0.1	0.2	0.1	0.1	0.1
tridecane	0.7	0.9	0.9	0.9	1.3	1.0	0.9	1.1
tetradecane	0.8	1.0	0.8	0.9	1.0	0.8	0.7	0.8
pentadecane	5.4	6.1	5.2	6.6	2.4	3.1	2.7	3.5
hexadecane	10.9	12.5	8.1	9.4	4.7	5.6	3.9	4.2
heptadecane	10.3	11.8	9.3	12.3	8.2	15.1	12.1	14.9
octadecane	19.3	23.2	13.3	16.1	17.4	26.0	16.7	17.1
				Alcohol				
hexadecanol	0.2	0.3	0.6	0.1	0.2	0.6	0.7	1.2
octadecanol	0.1	0.2	0.2	0.3	0.5	0.6	0.4	0.4
				Ester				
hexadecyl hexadecanoate	0.1	0.1	0.1	0.2	0.2	0.4	0.2	0.1
				Aldehyde				
hexadecanal	0.1	0.1	0.1	0.2	0.1	0.2	0.1	0.4

[a]Conditions: 300 °C, 40 bar P_{H2}, and 5 wt % oil concentration.

deoxygenation shown in Figure 6. The amount of the main products and byproducts formed, in terms of the percentage area under the GC curve, is shown in Figure 7 and Table 2. The deoxygenation of WCO was terminated with the removal of oxygen from fatty acids through three reactions: HDO, DCO, and DCO_2. However, the products included not only *n*-C_{15}−C_{18} but also low-molecular-weight *n*-C_5−C_{13}, indicating the cracking of some *n*-C_{15}−C_{18}, which converted large molecule normal alkanes into smaller molecule normal alkanes. For the deoxygenation catalyzed by the γ-Al_2O_3-supported $NiMoS_2$, the γ-Al_2O_3 carrier was acidic which facilitated the dissociation resulting in a higher small *n*-C_5−C_{13} yield compared with the unsupported $NiMoS_2$ catalyst.

With respect to the amount of Ni, for both the γ-Al_2O_3-supported and unsupported $NiMoS_2$ catalysts, the most efficient HDO was obtained with a Ni/(Ni + Mo) ratio of 0.2. The higher Ni content [Ni/(Ni + Mo) ratio of 0.3] led to a higher low-molecular-weight *n*-C_5−C_{13} content (Table 2) because the excessive Ni caused the catalyst to absorb so much H_2 that (i) hydrocracking took place converting macromolecules of normal alkanes to small molecules (*n*-C_5−C_{13}) and (ii) Ni had a greater chance to cover the pores of the catalyst, causing a decreased active site/substrate ratio in the catalyst. The latter effect also leads to the formation of alcohol and aldehyde byproducts due to the insufficient amount of active catalyst sites compared to the catalysts with a Ni/(Ni + Mo) ratio of 0.2.

With increasing the oil concentration to 10 wt %, the formation of byproducts, such as alcohols and aldehydes increased. The excess reactants (low catalytic site/substrate ratio) reduced the catalytic efficiency to form *n*-C_{15}−C_{18} resulting in the decreased HDO rate. Therefore, optimum conditions need to be adjusted to further transform the intermediates (alcohols) into the desired HCs in order to decrease the content of low-molecular-weight normal *n*-C_5−C_{13} in the fuel. In the oil refining process, *n*-C_6−C_{13} with a boiling point range of 65−170 °C (gasoline) can be separated by distillation and then used as motor fuel mixed with petroleum gasoline. The C_{10}−C_{14} fraction with a boiling point range of 170−250 °C (kerosene) can also be separated and mixed with petroleum kerosene for jet fuel.

3.4. Catalyst Characterization. The XRD patterns of the γ-Al_2O_3-supported and unsupported $NiMoS_2$ catalysts (0.2-$NiMoS_2$/γ-Al_2O_3, 0.3-$NiMoS_2$/γ-Al_2O_3, 0.2-$NiMoS_2$, and 0.3-$NiMoS_2$) are shown in Figure 8. The peak at 2θ of 14.4° is the basal plane (0 0 2) of MoS_2 and was decreased in the 0.2-$NiMoS_2$ and 0.3-$NiMoS_2$ catalysts. The wide dispersion peaks of the 0.2-$NiMoS_2$ catalyst implied a highly amorphous state (reduced crystallinity). For all catalysts, there is no separated Ni sulfide peak implying that most Ni were highly dispersed and incorporated in the form of Ni−Mo−S phases, which were hardly detected by the XRD technique. Additionally, separated Ni sulfides were observed for the Ni/(Ni + Mo) ratio above 0.43. This is probably due to the high loading amount of these metals and the NiS and Ni_3S_4 were formed.[35] This structure observed by XRD analysis would also be supported by TEM analysis. Representative TEM photographs of the supported and unsupported $NiMoS_2$ catalysts are shown in Figure 9, and their morphological properties are presented in Table 3. The 0.2-$NiMoS_2$ catalyst had a slab length of 10 nm and 5 layers (Figure 9a) of very small MoS_2 as a parallel dark line that was the (0 0 2) basal planes of crystalline MoS_2. Thus, the hydrothermal process with the Ni incorporation yielded the MoS_2 long slabs with curvature, implying the nanoparticle

https://doi.org/10.1021/acsomega.3c06188
ACS Omega 2023, 8, 40921−40933

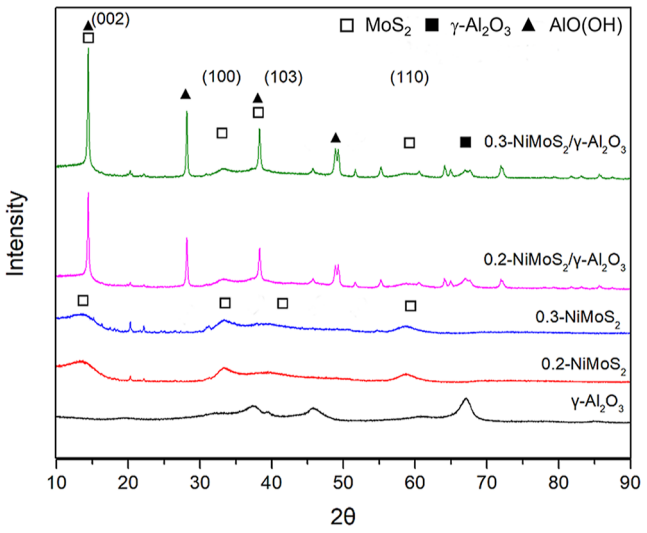

Figure 8. Representative XRD patterns of supported and unsupported $NiMoS_2$ catalysts.

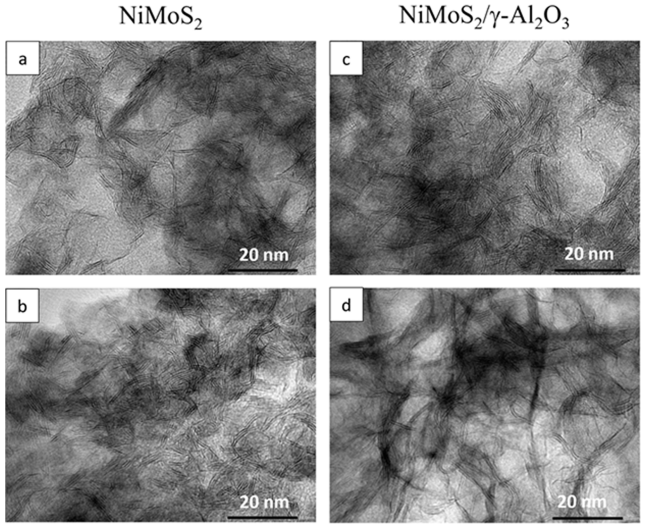

Figure 9. Representative TEM images (×600,000) of the (a) 0.2-$NiMoS_2$, (b) 0.3-$NiMoS_2$, (c) 0.2-$NiMoS_2/\gamma$-Al_2O_3, and (d) 0.3-$NiMoS_2/\gamma$-Al_2O_3 catalysts.

formation.[19] Hence, the $NiMoS_2$ catalyst also exhibited a multilayer fold structure with bending. The 0.2-$NiMoS_2$ and 0.3-$NiMoS_2$ catalysts had the same slab length (10 nm) and the number of stacks of 10 and 12, respectively (Table 3), indicating that the rim and edge sites with the addition of Ni promoter were the active sites for the deoxygenation reaction. The combination of XRD and TEM results confirmed that the 0.2-$NiMoS_2$ and 0.3-$NiMoS_2$ catalysts had similar structural and morphological properties. The morphology of the 0.2-$NiMoS_2$ was consistent with the observed high percentage yield of normal alkanes due to the hydrothermal process that the very small $NiMoS_2$ crystal as active sites would locate at the rim and edge of the stack for hydrogenation.

For the XRD patterns of the γ-Al_2O_3-supported catalyst, the 0.2-$NiMoS_2/\gamma$-Al_2O_3 and 0.3-$NiMoS_2/\gamma$-Al_2O_3 catalysts had a boehmite alumina structure [γ-AlO(OH)] as the γ-Al_2O_3 can react with water to form boehmite during the catalyst preparation step in the ATTM hydrothermal method. In addition, the peaks at a 2θ of 14.4 and 38°, an overlap between the AlO(OH) peak and the MoS_2 peak, were expected and the peaks of γ-Al_2O_3 and AlO(OH) at the (1 0 0) and (1 1 0) planes represented their agglomeration at a high density. From TEM photographs of the supported $NiMoS_2$ (Figure 9) and their morphological properties (Table 3), when γ-Al_2O_3 was added to form the 0.2-$NiMoS_2/\gamma$-Al_2O_3 catalyst, the slab length (12.3 nm) and the number of layers (seven layers) both increased slightly but the number of stacks increased markedly from 10 to 22 (Figure 9c). The 0.3-$NiMoS_2$ (Figure 9b) and 0.3-$NiMoS_2/\gamma$-Al_2O_3 (Figure 9d) catalysts had the same number of layers (five), but the latter had a slightly longer slab length and more stacks (18), although they were both broadly similar to the respective catalysts with Ni/(Ni + Mo) ratios of 0.2 and 0.3. Fortunately, the 0.2-$NiMoS_2/\gamma$-Al_2O_3 had the highest number of stacks and number of layers, resulting in an increase in the edge and rim positions as active sites for deoxygenation, where the substrate would undergo HDO producing a higher amount of C_{13}–C_{18} alkane products. The morphology of the 0.2-$NiMoS_2/\gamma$-Al_2O_3 catalyst was consistent with the observed high percentage yield of normal alkanes due to the hydrothermal process that the $NiMoS_2$ crystal would be recrystallized and dispersed on the surface of Al_2O_3.

The physical properties of the γ-Al_2O_3-supported and unsupported $NiMoS_2$ catalysts, the S_{BET}, V_p, and pore diameter, are presented in Table 4. From the N_2 adsorption–desorption isotherms (Figure 10), the supported and unsupported $NiMoS_2$ catalysts both exhibited a type-IV isotherm, implying a mesopore structure. The pore diameter and surface area of unsupported 0.2-$NiMoS_2$ and 0.3-$NiMoS_2$ catalysts were 5.84 and 5.31 nm and 214.7 and 188.5 m^2/g, respectively, supported by similar N_2 adsorption–desorption

Table 4. Physicochemical Properties of the Supported and Unsupported $NiMoS_2$ Catalysts

catalyst	S_{BET} (m^2/g)	V_p (cm^3/g)	pore diameter (nm)	total acidity (mmol/g)
0.2-$NiMoS_2$	214.7	0.39	5.84	0.065
0.3-$NiMoS_2$	188.5	0.29	5.31	0.153
0.2-$NiMoS_2/\gamma$-Al_2O_3	104.5	0.23	6.99	0.120
0.3-$NiMoS_2/\gamma$-Al_2O_3	81.1	0.17	9.35	0.328
γ-Al_2O_3	131.2	0.24	5.28	0.396

Table 3. Morphological Character of the Supported and Unsupported $NiMoS_2$ Catalysts

				element (wt %)				
catalyst	slab length (nm)	number of stacks	number of layers	Mo	Ni	S	Al	Ni/(Ni + Mo)
0.2-$NiMoS_2$	10	10	5	49.6	3.5	46.9	n.a.	0.10
0.3-$NiMoS_2$	10	12	5	54.4	4.6	41.0	n.a.	0.12
0.2-$NiMoS_2/\gamma$-Al_2O_3	12.3	22	7	43.2	3.3	39.4	14.1	0.11
0.3-$NiMoS_2/\gamma$-Al_2O_3	12	18	5	39.5	3.7	38.1	18.7	0.13

https://doi.org/10.1021/acsomega.3c06188
ACS Omega 2023, 8, 40921–40933

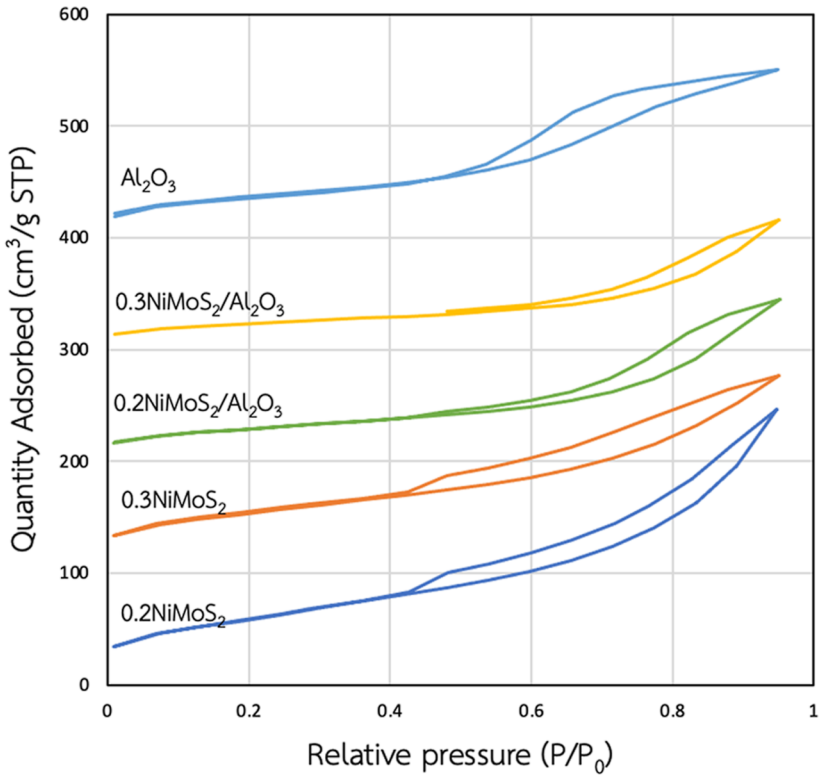

Figure 10. Representative N_2 adsorption and desorption isotherms of the supported and unsupported $NiMoS_2$ catalysts.

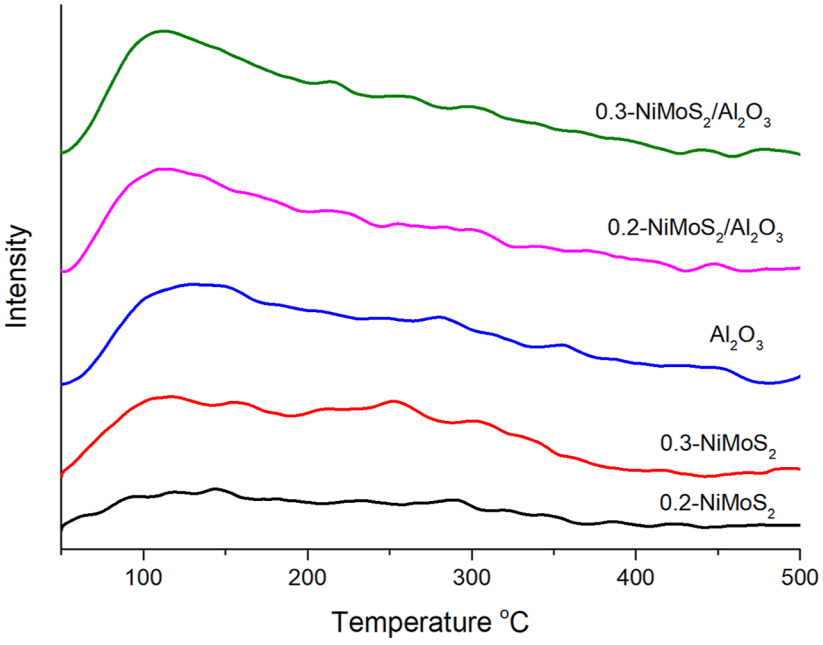

Figure 11. Representative NH_3-TPD profiles of the supported and unsupported $NiMoS_2$ catalysts.

isotherms (Figure 10). Whereas the pore diameter and surface area of supported 0.2-$NiMoS_2/\gamma$-Al_2O_3 and 0.3-$NiMoS_2/\gamma$-Al_2O_3 catalysts were increased to 6.99 and 9.35 nm and decreased to 104.5 and 81.3 m^2/g, respectively. Thus, binding of $NiMoS_2$ to γ-Al_2O_3 had an influence on the increased pore size and decreased surface area of the catalyst. Apparently, the small pore diameter and high S_{BET} of 0.2-$NiMoS_2$ and 0.3-$NiMoS_2$ catalysts and the large pore diameter and low S_{BET} of supported 0.2-$NiMoS_2/\gamma$-Al_2O_3 and 0.3-$NiMoS_2/\gamma$-Al_2O_3 catalysts corresponded to the difference in N_2 adsorption−desorption isotherms of unsupported and supported catalysts (Figure 10). For the supported and unsupported catalysts, the S_{BET} decreased as follows (highest to lowest): 0.2-$NiMoS_2$ > 0.3-$NiMoS_2$ > 0.2-$NiMoS_2/\gamma$-Al_2O_3 > 0.3-$NiMoS_2/\gamma$-Al_2O_3. The supported $NiMoS_2/\gamma$-Al_2O_3 catalyst had a higher pore size (than that of the unsupported $NiMoS_2$). The 0.3-$NiMoS_2/\gamma$-Al_2O_3 catalyst had a lower S_{BET} (81.1 m^3/g) and V_p (0.17 cm^3/g) than did the 0.2-$NiMoS_2/\gamma$-Al_2O_3, implying that the lower

https://doi.org/10.1021/acsomega.3c06188
ACS Omega 2023, 8, 40921−40933

surface area resulted in the low reactivity of the catalyst in accordance with the lower C_{13}−C_{18} yield obtained in HDO (Table 1). This low activity of the 0.3-$NiMoS_2/\gamma$-Al_2O_3 catalyst can be explained by the low surface area and the Ni agglomerate, resulting in decreasing Ni dispersity that interfered with the HDO reaction.

From the NH_3-TPD profiles of the supported and unsupported $NiMoS_2$ catalysts, as shown in Figure 11, the acid sites in the catalyst were divided into weak, medium, and strong acid sites based upon the NH_3-TPD profiles as 50−150, 150−300, and above 300 °C, respectively. In Table 4, the unsupported 0.2-$NiMoS_2$ catalyst exhibited a desorption peak at around 100−400 °C and had the lowest total acidity (0.065 mmol/g), while the supported 0.2-$NiMoS_2/\gamma$-Al_2O_3 catalyst had a higher total acid content of 0.120 mmol/g catalyst. Similarly, the 0.3-$NiMoS_2$ and 0.3-$NiMoS_2/\gamma$-Al_2O_3 catalysts exhibited a large desorption peak and had an increased total acidity (0.153 and 0.328 mmol/g, respectively). Because γ-Al_2O_3 has a Lewis acidic character and a total acidity of 0.396 mmol/g, the supported $NiMoS_2/\gamma$-Al_2O_3 catalysts possessed higher weak and medium acid sites. The total acidity sequence of the supported and unsupported $NiMoS_2$ catalysts is as follows (highest to lowest): 0.3-$NiMoS_2/\gamma$-Al_2O_3 > 0.3-$NiMoS_2$ > 0.2-$NiMoS_2/\gamma$-Al_2O_3 > 0.2-$NiMoS_2$.

In addition, the acidity of the catalyst was higher due to the Lewis acidity of Ni, causing the peaks for the weak and medium acid positions to increase. The acidity of the 0.3-$NiMoS_2$ catalyst was higher than that of 0.2-$NiMoS_2$. Therefore, the Ni promoter added to the $NiMoS_2$ catalyst for the HDO reaction must be in the appropriate ratio. A Ni/(Ni + Mo) ratio higher than 0.2 made the catalyst more acidic and enhanced the hydrocracking with a decrease in the n-C_{15}−C_{18} yield.

The γ-Al_2O_3 support was also used to increase the number of slab stacks in the catalyst on which the substrate to react on. A good reactivity requires a proper dosage to prevent the catalyst from being too acidic and degrading the main products (n-C_{15}−C_{18} alkanes). The efficient catalyst should have the appropriate amount of Ni, γ-Al_2O_3 (20 wt %) and be prepared via the hydrothermal method to give a suitable catalyst morphology with a good dispersion of Ni atoms at the rim and edge active sites.

In summary of the activity-selectivity and characterization results, the C_{14}−C_{18} yield (47−58%) from WCO deoxygenation using four $NiMoS_2$ catalysts was controlled by the XRD peak pattern that showed the similarity of 0.2-$NiMoS_2$ and 0.3-$NiMoS_3$, and the similarity of 0.2-$NiMoS_2/\gamma$-Al_2O_3 and 0.3-$NiMoS_2/\gamma$-Al_2O_3 catalyst. Meanwhile, the C_{14}−C_{18} yield from deoxygenation using four $NiMoS_2$ catalysts was also controlled by TEM images that all showed very small MoS_2 layers and stacks only different stack numbers (0.2-$NiMoS_2$ and 0.3-$NiMoS_3$ had 10 and 12 stacks, 0.2-$NiMoS_2/\gamma$-Al_2O_3 and 0.3-$NiMoS_2/\gamma$-Al_2O_3 had 22 and 18 stacks, respectively). The supported $NiMoS_2$ prepared by the hydrothermal method could give the active rim and edge sites for hydrogenation while the supported NiMo and $NiMoS_2$ catalysts prepared by impregnation did not show the MoS_2 layer.[28] In addition, the N_2 adsorption−desorption and acidity of catalysts had a more pronounced effect (balance of surface area and acidity) on C_{14}−C_{18} yield that two efficient catalysts, 0.2-$NiMoS_2$ with a high surface area and low acidity and 0.2-$NiMoS_2/\gamma$-Al_2O_3 catalyst with a lower surface area and higher acidity, gave a C_{14}−C_{18} yield of 55−58%.

4. CONCLUSIONS

The supported 0.2-$NiMoS_2/\gamma$-Al_2O_3 catalysts prepared via the hydrothermal method had a sufficiently good HDO activity owing to a high MoS_2 layer and a high number of exposed edge and rim sites. The optimum conditions for the HDO were 300 °C and 40 bar of initial P_{H_2} under which the highest yield of n-alkane was obtained. For the deoxygenation of WPO over the 0.2-$NiMoS_2/\gamma$-Al_2O_3 catalyst, a total C_{14}−C_{18} alkane yield of 56.4% (in the diesel range) and n-C_{18}/C_{17} and n-C_{16}/C_{15} ratios of 1.9 and 2.2, respectively, were achieved. The deoxygenation of WSBO over the 0.2-$NiMoS_2/\gamma$-Al_2O_3 catalyst gave a total C_{14}−C_{18} alkane yield of 58.0% and n-C_{18}/n-C_{17} and n-C_{16}/n-C_{15} ratios of 1.7 and 1.8, respectively. This implies that the deoxygenation of both WCOs- favored HDO over DCO and DCO_2.

■ ASSOCIATED CONTENT

Supporting Information

The Supporting Information is available free of charge at https://pubs.acs.org/doi/10.1021/acsomega.3c06188.

Effect of reaction time and oil concentration on deoxygenation of FPO, WPO, FSBO, and WSBO, representative GC/MS chromatogram of products, and comparison of unsupported and γ-Al_2O_3-supported $NiMoS_2$ catalysts (PDF)

■ AUTHOR INFORMATION

Corresponding Author

Pattarapan Prasassarakich − *Department of Chemical Technology, Faculty of Science, Chulalongkorn University, Bangkok 10330, Thailand; Center of Excellence on Petrochemical and Materials Technology (PETROMAT), Chulalongkorn University, Bangkok 10330, Thailand;* orcid.org/0000-0002-5554-7658; Email: ppattara@chula.ac.th

Authors

Dechpol Prangklang − *Department of Chemical Technology, Faculty of Science, Chulalongkorn University, Bangkok 10330, Thailand; Center of Excellence on Petrochemical and Materials Technology (PETROMAT), Chulalongkorn University, Bangkok 10330, Thailand*

Dusadee Tumnantong − *Department of Chemical Technology, Faculty of Science, Chulalongkorn University, Bangkok 10330, Thailand*

Boonyawan Yoosuk − *Clean Fuel Technology and Advanced Chemistry Research Team, National Energy Technology Center, National Science and Technology Development Agency, Pathum, Thani 12120, Thailand;* orcid.org/0000-0003-2107-1150

Chawalit Ngamcharussrivichai − *Department of Chemical Technology, Faculty of Science, Chulalongkorn University, Bangkok 10330, Thailand; Center of Excellence on Petrochemical and Materials Technology (PETROMAT) and Center of Excellence in Catalysis for Bioenergy and Renewable Chemicals (CBRC), Faculty of Science, Chulalongkorn University, Bangkok 10330, Thailand;* orcid.org/0000-0002-5621-8880

Complete contact information is available at: https://pubs.acs.org/10.1021/acsomega.3c06188

https://doi.org/10.1021/acsomega.3c06188
ACS Omega 2023, 8, 40921−40933

Author Contributions

D.P.: formal analysis, investigation, and writing—original draft preparation. D.T.: supervision, and writing—review and editing. B.Y.: supervision and writing—review and editing. C.N.: supervision and writing—review and editing. P.P.: conceptualization, methodology, supervision, writing—review and editing, funding acquisition, and resources.

Funding

The Center of Excellence on Petrochemical and Materials Technology (PETROMAT) and the National Energy Technology Center (ENTEC), National Science and Technology Development Agency (NSTDA).

Notes

The authors declare no competing financial interest.

■ ACKNOWLEDGMENTS

The authors gratefully acknowledge the support from the Center of Excellence on Petrochemical and Materials Technology (PETROMAT) and the National Energy Technology Center (ENTEC), National Science and Technology Development Agency (NSTDA). We thank Dr. Robert Butcher for editing the article and making suggestions.

■ REFERENCES

(1) Mohamed, R. K. M. K.; Ramendran, C.; Yacob, P. A study on turnover intention in fast food industry: Employees' fit to the organizational culture and the important of their commitment. *Int. J. Acad. Res. Bus. Soc. Sci.* **2012**, *2* (5), 2222−6990. https://api.semanticscholar.org/CorpusID:11050959

(2) Mandolesi de Araújo, C. D.; de Andrade, C. C.; de Souza e Silva, E.; Dupas, F. A. Biodiesel production from used cooking oil: A review. *Renew. Sustain. Energy Rev.* **2013**, *27*, 445−452.

(3) Liu, Q.; Zuo, H.; Zhang, Q.; Wang, T.; Ma, L. Hydrodeoxygenation of palm oil to hydrocarbon fuels over Ni/SAPO-11 catalysts. *Chin. J. Catal.* **2014**, *35* (5), 748−756.

(4) Wang, H.-Y.; Jiao, T.-T.; Li, Z.-X.; Li, C.-S.; Zhang, S.-J.; Zhang, J.-L. Study on palm oil hydrogenation for clean fuel over Ni-Mo-W/γ-Al_2O_3-ZSM-5 catalyst. *Fuel Process. Technol.* **2015**, *139*, 91−99.

(5) Yani, F. T.; Husin, H.; Darmadi; Muhammad, S.; Abnisa, F.; Nurhazanah; Nasution, F.; Erdiwansyah. Palm oil hydrodeoxygenation into green diesel over NiO/$NbOPO_4$ catalyst: A novel approach of synthesizing $NbOPO_4$ from $NbCl_5$. *J. Clean. Prod.* **2022**, *354*, 131704.

(6) Veriansyah, B.; Han, J. Y.; Kim, S. K.; Hong, S.-A.; Kim, Y. J.; Lim, J. S.; Shu, Y. W.; Oh, S. G.; Kim, J. Production of renewable diesel by hydroprocessing of soybean oil: Effect of catalysts. *Fuel* **2012**, *94*, 578−585.

(7) Šimáček, P.; Kubička, D.; Šebor, G.; Pospíšil, M. Fuel properties of hydroprocessed rapeseed oil. *Fuel* **2010**, *89* (3), 611−615.

(8) Kubička, D.; Kaluža, L. Deoxygenation of vegetable oils over sulfided Ni, Mo and NiMo catalysts. *Appl. Catal., A* **2010**, *372* (2), 199−208.

(9) Huber, G. W.; O'Connor, P.; Corma, A. Processing biomass in conventional oil refineries: Production of high quality diesel by hydrotreating vegetable oils in heavy vacuum oil mixtures. *Appl. Catal., A* **2007**, *329*, 120−129.

(10) Chen, J.; Yang, Y.; Shi, H.; Li, M.; Chu, Y.; Pan, Z.; Yu, X. Regulating product distribution in deoxygenation of methyl laurate on silica-supported Ni-Mo phosphides: Effect of Ni/Mo ratio. *Fuel* **2014**, *129*, 1−10.

(11) Wang, J.; Bi, P.; Zhang, Y.; Xue, H.; Jiang, P.; Wu, X.; Liu, J.; Wang, T.; Li, Q. Preparation of jet fuel range hydrocarbons by catalytic transformation of bio-oil derived from fast pyrolysis of straw stalk. *Energy* **2015**, *86*, 488−499.

(12) Zhang, H.; Lin, H.; Wang, W.; Zheng, Y.; Hu, P. Hydroprocessing of waste cooking oil over a dispersed nano catalyst: Kinetics study and temperature effect. *Appl. Catal., B* **2014**, *150*−*151*, 238−248.

(13) Zhang, M.; Xiang, L.; Fan, G.; Yang, L.; Li, F. Unveiling the role of surface basic sites on ruthenium-based nanocatalysts for enhanced hydrodeoxygenation of guaiacol. *Mol. Catal.* **2022**, *533*, 112794.

(14) Kaewchada, A.; Akkarawatkhoosith, N.; Bunpim, D.; Bangjang, T.; Ngamcharussrivichai, C.; Jaree, A. Production of bio-hydrogenated diesel from palm oil using Rh/HZSM-5 in a continuous mini fixed-bed reactor. *Chem. Eng. Process.* **2021**, *168*, 108586.

(15) Zhou, L.; Lawal, A. Kinetic study of hydrodeoxygenation of palmitic acid as a model compound for microalgae oil over Pt/γ-Al_2O_3. *Appl. Catal., A* **2017**, *532*, 40−49.

(16) Duan, J.; Han, J.; Sun, H.; Chen, P.; Lou, H.; Zheng, X. Diesel-like hydrocarbons obtained by direct hydrodeoxygenation of sunflower oil over Pd/Al-SBA-15 catalysts. *Catal. Commun.* **2012**, *17*, 76−80.

(17) Ruangudomsakul, M.; Osakoo, N.; Wittayakun, J.; Keawkumay, C.; Butburee, T.; Youngjan, S.; Faungnawakij, K.; Poo-arporn, Y.; Kidkhunthod, P.; Khemthong, P. Hydrodeoxygenation of palm oil to green diesel products on mixed-phase nickel phosphides. *Mol. Catal.* **2022**, *523*, 111422.

(18) Srifa, A.; Faungnawakij, K.; Itthibenchapong, V.; Viriya-empikul, N.; Charinpanitkul, T.; Assabumrungrat, S. Production of bio-hydrogenated diesel by catalytic hydrotreating of palm oil over $NiMoS_2$/γ-Al_2O_3 catalyst. *Bioresour. Technol.* **2014**, *158*, 81−90.

(19) Yoosuk, B.; Sanggam, P.; Wiengket, S.; Prasassarakich, P. Hydrodeoxygenation of oleic acid and palmitic acid to hydrocarbon-like biofuel over unsupported Ni-Mo and Co-Mo sulfide catalysts. *Renew. Energy* **2019**, *139*, 1391−1399.

(20) Yoosuk, B.; Tumnantong, D.; Prasassarakich, P. Unsupported MoS_2 and $CoMoS_2$ catalysts for hydrodeoxygenation of phenol. *Chem. Eng. Sci.* **2012**, *79*, 1−7.

(21) Sankaranarayanan, T. M.; Banu, M.; Pandurangan, A.; Sivasanker, S. Hydroprocessing of sunflower oil-gas oil blends over sulfided Ni-Mo-Al-zeolite beta composites. *Bioresour. Technol.* **2011**, *102* (22), 10717−10723.

(22) Popov, A.; Kondratieva, E.; Mariey, L.; Goupil, J. M.; El Fallah, J.; Gilson, J.-P.; Travert, A.; Maugé, F. Bio-oil hydrodeoxygenation: Adsorption of phenolic compounds on sulfided (Co)Mo catalysts. *J. Catal.* **2013**, *297*, 176−186.

(23) Kim, T.-S.; Oh, S.; Kim, J.-Y.; Choi, I.-G.; Choi, J. W. Study on the hydrodeoxygenative upgrading of crude bio-oil produced from woody biomass by fast pyrolysis. *Energy* **2014**, *68*, 437−443.

(24) Itthibenchapong, V.; Chakthranont, P.; Sattayanon, C.; Butburee, T.; Faungnawakij, K.; Namuangruk, S. Understanding the promoter effect of bifunctional (Pt, Ni, Cu)-MoO_{3-x}/TiO_2 catalysts for the hydrodeoxygenation of p-cresol: A combined DFT and experimental study. *Appl. Surf. Sci.* **2021**, *547*, 149170.

(25) Hongloi, N.; Prapainainar, P.; Seubsai, A.; Sudsakorn, K.; Prapainainar, C. Nickel catalyst with different supports for green diesel production. *Energy* **2019**, *182*, 306−320.

(26) Itthibenchapong, V.; Srifa, A.; Kaewmeesri, R.; Kidkhunthod, P.; Faungnawakij, K. Deoxygenation of palm kernel oil to jet fuel-like hydrocarbons using Ni-MoS_2/γ-Al_2O_3 catalysts. *Energy Convers. Manage.* **2017**, *134*, 188−196.

(27) Pongsiriyakul, K.; Kiatkittipong, W.; Kiatkittipong, K.; Laosiripojana, N.; Faungnawakij, K.; Adhikari, S.; Assabumrungrat, S. Alternative Hydrocarbon Biofuel Production via Hydrotreating under a Synthesis Gas Atmosphere. *Energy Fuel.* **2017**, *31* (11), 12256−12262.

(28) Aiamsiri, P.; Tumnantong, D.; Yoosuk, B.; Ngamcharussrivichai, C.; Prasassarakich, P. Biohydrogenated diesel from palm oil deoxygenation over unsupported and γ-Al_2O_3 supported Ni-Mo catalysts. *Energy Fuel.* **2021**, *35* (18), 14793−14804.

(29) Miao, C.; Marin-Flores, O.; Davidson, S. D.; Li, T.; Dong, T.; Gao, D.; Wang, Y.; Garcia-Pérez, M.; Chen, S. Hydrothermal catalytic deoxygenation of palmitic acid over nickel catalyst. *Fuel* **2016**, *166*, 302−308.

https://doi.org/10.1021/acsomega.3c06188
ACS Omega 2023, 8, 40921−40933

(30) Lee, D.-S.; Noh, B.-S.; Bae, S.-Y.; Kim, K. Characterization of fatty acids composition in vegetable oils by gas chromatography and chemometrics. *Anal. Chim. Acta* **1998**, *358* (2), 163−175.
(31) Satyarthi, J. K.; Chiranjeevi, T.; Gokak, D. T.; Viswanathan, P. S. An overview of catalytic conversion of vegetable oils/fats into middle distillates. *Catal. Sci. Technol.* **2013**, *3* (1), 70−80.
(32) Burimsitthigul, T.; Yoosuk, B.; Ngamcharussrivichai, C.; Prasassarakich, P. Hydrocarbon biofuel from hydrotreating of palm oil over unsupported Ni-Mo sulfide catalysts. *Renew. Energy* **2021**, *163*, 1648−1659.
(33) Yoosuk, B.; Tumnantong, D.; Prasassarakich, P. Amorphous unsupported Ni-Mo sulfide prepared by one step hydrothermal method for phenol hydrodeoxygenation. *Fuel* **2012**, *91* (1), 246−252.
(34) Pugazhendhi, A.; Alagumalai, A.; Mathimani, T.; Atabani, A. E. Optimization, kinetic and thermodynamic studies on sustainable biodiesel production from waste cooking oil: An Indian perspective. *Fuel* **2020**, *273*, 117725.
(35) Yoosuk, B.; Song, C.; Kim, J. H.; Ngamcharussrivichai, C.; Prasassarakich, P. Effects of preparation conditions in hydrothermal synthesis of highly active unsupported NiMo sulfide catalysts for simultaneous hydrodesulfurization of dibenzothiophene and 4,6-dimethyldibenzothiophene. *Catal. Today* **2010**, *149* (1−2), 52−61.

https://doi.org/10.1021/acsomega.3c06188
ACS Omega 2023, 8, 40921−40933